

$O(^3P)+CO_2$ scattering cross sections at superthermal collision energies for planetary aeronomy

M. Gacesa^{1,2}, R. J. Lillis³, and K. J. Zahnle²

¹Bay Area Environmental Research Institute, Moffett Field, California, USA

²Space Science Division, NASA Ames Research Center, MS 245-3, Moffett Field, California, USA

³Space Sciences Laboratory, University of California, Berkeley, California, USA

Key Points:

- Velocity-dependent quantum mechanical state-to-state scattering cross sections for $O(^3P)+H_2$ were calculated from first principles.
- Elastic cross sections at collision energies $E > 3.5$ eV more than 50% smaller than previous estimates.
- Higher photochemical oxygen escape rate and water loss from Mars than predicted by models relying on mass-scaling cross sections expected.

arXiv:1906.11368v1 [astro-ph.EP] 26 Jun 2019

Corresponding author: M. Gacesa, marko.gacesa@nasa.gov

Abstract

We report new elastic and inelastic cross sections for $O(^3P)+CO_2$ scattering at collision energies from 0.03 to 5 eV, of major importance to O escape from Mars, Venus, and CO_2 -rich atmospheres. The cross sections were calculated from first principles using three newly constructed ab-initio potential energy surfaces correlating to the lowest energy asymptote of the complex. The surfaces were restricted to a planar geometry with the CO_2 molecule assumed to be in linear configuration fixed at equilibrium. Quantum-mechanical coupled-channel formalism with a large basis set was used to compute state-to-state integral and differential cross sections for elastic and inelastic $O(^3P)+CO_2$ scattering between all pairs of rotational states of CO_2 molecule. The elastic cross sections are 35% lower at 0.5 eV and more than 50% lower at 4+ eV than values commonly used in studies of processes in upper and middle planetary atmospheres of Mars, Earth, Venus, and CO_2 -rich planets. Momentum transfer cross sections, of interest for energy transport, were found to be lower than predicted by mass-scaling.

Plain Language Summary

Understanding oxygen escape to space is a key to understanding ancient water reservoirs on Mars and evolution of the martian atmosphere over time. More broadly, this is true of all planets with CO_2 atmospheres, including Venus. On Mars, there are two modes of atmospheric escape: thermal evaporation and non-thermal. Thermal evaporation is relevant only to hydrogen, the lightest element. However, since water escapes to space as its components, hydrogen and oxygen, the much heavier oxygen acts as a 'bottleneck'. Oxygen escapes through non-thermal processes. Here, we computed physical quantities called 'O- CO_2 collision cross sections' that determine how likely are escaping oxygen atoms to collide with CO_2 molecules and lose enough energy to slow down so that they can no longer escape. The cross sections for this particular process are usually estimated from simpler atom-atom collisions. Our results show that such estimates tend to overestimate the energy loss by about a factor of two. Thus, we expect that more oxygen could have escaped from Mars than previously believed and that more water could have been present on Mars in its ancient history. This study was conducted 'from first principles', or directly from fundamental physical theory without additional fitted parameters.

1 Introduction

Understanding oxygen escape to space is a key to understanding evolution of the martian atmosphere. To first approximation, atomic hydrogen and oxygen escape from Mars are linked together. At present, H and O escape are directly related to water escape, as there is no pronounced evidence of excess of either species accumulating in the atmosphere. The global time-integrated rate of H escape is, therefore, equal to twice the global time-integrated O escape rate. While hydrogen escapes easily from Mars, mainly through thermal Jeans escape mechanism, atomic O escapes with difficulty due to its high mass (Hunten & Donahue, 1976). As a result, it is the O escape rate that is limiting and its escape mechanism determines the loss of water and, consequently, plays the biggest role in determining the atmospheric evolution on Mars (Liu & Donahue, 1976; Hunten & Donahue, 1976; Lammer et al., 2003; Zahnle et al., 2008). Curiously, the same 2:1 ratio is inferred in H-to-O escape rates from Venus (Liu & Donahue, 1975), suggesting principal importance of O escape at Venus, and for Venusian atmospheric evolution.

The mechanism driving the O escape from Mars is largely photochemical (Jakosky et al., 2018). In its upper atmospheres, photodissociation of molecular O_2 , O_3 (ozone),

CO₂, and CO by solar ultraviolet (UV) photons produces superthermal atomic oxygen in the ground state, O(³P), as well as electronically excited O(¹D) and O(¹S). Photodissociative recombination of O₂⁺ and CO₂⁺ molecular ions with electrons preferentially produces superthermal O(³P), with kinetic energies up to 3.5 eV, capable of overcoming Mars' gravitational potential and escaping to space (Fox & Hać, 2009). This mechanism, called photochemical escape, appears to be the dominant non-thermal atmospheric escape mechanism presently active on Mars (Lillis et al., 2017). Superthermal O atoms also drive escape of other atmospheric species, such as Ar, He, H₂, OH and H₂O, through kinetic energy transfer in collisions, contributing to additional non-thermal atmospheric loss (Leblanc et al., 2019). The non-thermal atmospheric escape rates strongly depend on the attenuation of the hot O flux in the Martian upper atmosphere, which mainly depends on O(³P)+CO₂ scattering properties at superthermal energies.

Owing to the fact that CO₂ is a greenhouse gas as well as an important coolant (via emission at 15 μm line) in the middle and upper atmospheres of terrestrial planets (Sharma & Wintersteiner, 1990), the O(³P)+CO₂ scattering has been a subject of numerous investigations. Early theoretical work focused mainly on energy transfer to and from specific vibrational states (Bass, 1974; Billing & Clary, 1983; Schatz & Redmon, 1981; Mullaney Harvey, 1982; Garrett, 1984). They found that the energy transfer could be described well using impulse approximation in the superthermal regime, similar to collisions of CO₂ with noble gas atoms (Suzukawa Jr et al., 1978). More recent studies covered the collision energies corresponding to temperatures 150 K ≤ T ≤ 550 K, of interest in terrestrial atmosphere, and focused on understanding collisional de-excitation (quenching) of vibrationally excited CO₂ by the O atoms, namely O(³P)+CO₂(01¹0) → O(³P) + CO₂(00⁰0), as well as energy transfer between internal rotational and vibrational degrees of freedom (Castle et al., 2006; de Lara-Castells et al., 2006, 2007; Castle et al., 2012; Feofilov et al., 2012; Cecchini & Castle, 2015).

Yeung et al. (2012) experimentally and theoretically investigated O(³P)+CO₂ scattering at superthermal energies with isotopically labeled ¹²C¹⁸O₂. In a crossed molecular beam experiment at 98.8 kcal/mol (4.28 eV), they measured elastic and inelastic scattering of ¹⁶O(³P)+¹²C¹⁶O₂, as well as rate constants for two reactions: isotope exchange and O atom abstraction. They also performed quasi-classical trajectory (QCT) calculations for collision energies from 1 eV to 6.5 eV. However, the study of Yeung et al. (2012) was focused on understanding the role of transient molecular states in reactive scattering processes, in particular the oxygen isotope exchange and its role in atomic oxygen cycling via CO₂ in the Earth's atmosphere, rather than on constructing detailed elastic and inelastic scattering cross sections at superthermal energies for purposes of planetary aeronomy.

In the absence of targeted studies, in planetary aeronomy O(³P)+CO₂ scattering cross sections are commonly estimated by mass-scaling from systems whose scattering properties at superthermal energies are known better, including O+O (Kharchenko et al., 2000), O+N₂ (Balakrishnan et al., 1998), Ar+H₂ (Uudus et al., 2005), and O+H₂ (Gacesa & Kharchenko, 2014), or from general properties of atom-molecule cross sections at high collision energies (Lewkow & Kharchenko, 2014). For example, quantifying photochemical escape of oxygen from Mars (Cipriani et al., 2007; Fox & Hać, 2009) and interpreting data from Mars Atmosphere and Volatile Evolution (MAVEN) mission (Lee, Combi, Tenishev, Bougher, & Lillis, 2015; Lee, Combi, Tenishev, Bougher, Deighan, et al., 2015; Lillis et al., 2015, 2017; Leblanc et al., 2017; Amerstorfer et al., 2017) and collisionally-induced escape processes driven by superthermal O atoms (Bovino et al., 2011; Lammer, 2013; Gacesa et al., 2012; Lewkow & Kharchenko, 2014; Gacesa et al., 2017; Shematovich, 2017), relied on mass-scaled cross sections specifically adapted for planetary aeronomy (Fox & Hać, 2014, 2018). These studies

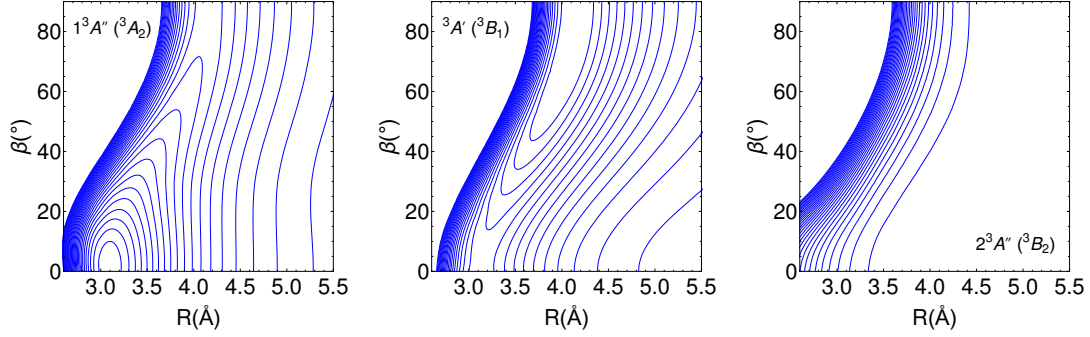


Figure 1. Contour plots of the three energetically-lowest potential energy surfaces for the $\text{CO}_2\text{-O}(^3P)$ complex: $1^3A''$ (left), $3^3A'$ (middle), $2^3A''$ (right). The CO_2 molecule is kept at equilibrium in linear geometry.

recognized that accurate $\text{O}(^3P)+\text{CO}_2$ cross sections are needed to reduced the uncertainties in present day atmospheric escape from Mars and estimates of its primordial water inventory (Lillis et al., 2017; Jakosky et al., 2018).

Here, we present the results of a theoretical study of $\text{O}(^3P) + \text{CO}_2(j) \rightarrow \text{O}(^3P) + \text{CO}_2(j')$ elastic and inelastic quantum-mechanical scattering cross sections at collision energies between 0.03 and 5 eV. In addition, we present differential and momentum transfer cross sections, of interest for hot atomic oxygen transport and energy transfer at non-thermal-equilibrium conditions in middle and upper planetary atmospheres (Kao et al., 2019). Our newly constructed cross sections are of particular interest to Mars aeronomy missions, such as NASA’s MAVEN mission (Jakosky et al., 2015) and ESA’s Trace Gas Orbiter (TGO), as well as to future Venus missions (Kallio et al., 2011). Moreover, velocity-dependent $\text{O}(^3P) + \text{CO}_2(j)$ cross sections enter models seeking to explain variations in the mass-independent fractionation (MIF) of stratospheric carbon dioxide (Thiemens et al., 1995; Wiegel et al., 2013) used to estimate carbon cycle reservoir size and rates of exchange for precise quantification of anthropogenic CO_2 and its effects on Earth’s climate (Thiemens et al., 2014).

2 Theoretical Methods

2.1 Electronic Structure of $\text{O}(^3P)\text{-CO}_2$ complex

We first constructed *ab-initio* potential energy surfaces (PESs) for three energetically lowest electronic states of the CO_3 complex that correlate to the $\text{O}(^3P)$ asymptote. We assumed that the CO_2 molecule is in its ground vibrational state, $\text{CO}_2(v_s v_b^l v_a) = \text{CO}_2(00^0 0)$, where $v_s = 0$, $v_b^l = 0$ and $v_a = 0$ are symmetric, bending, and asymmetric vibrational modes, respectively. Non-vibrating $\text{CO}_2(00^0 0)$ is linear and symmetric, with the C-O internuclear distance, r_{CO} , fixed at the equilibrium potential obtained by geometry optimization (de Lara-Castells et al., 2006).

With this assumption, the rotational symmetry with respect to the OCO internuclear axis is preserved and the three PESs of the CO_3 complex can be described in 2D planar geometry in terms of distance R , defined as the internuclear distance between the impacting $\text{O}(^3P)$ atom and the C atom of the CO_2 molecule, and the angle $0^\circ \leq \beta \leq 90^\circ$ between the CO_2 internuclear axis and the vector R . The symmetry group of the system will be at least C_S and depend on the angle of approach β . The lowest three PESs consist of a single $3^3A'$ and two $3^3A''$ electronic states. The special

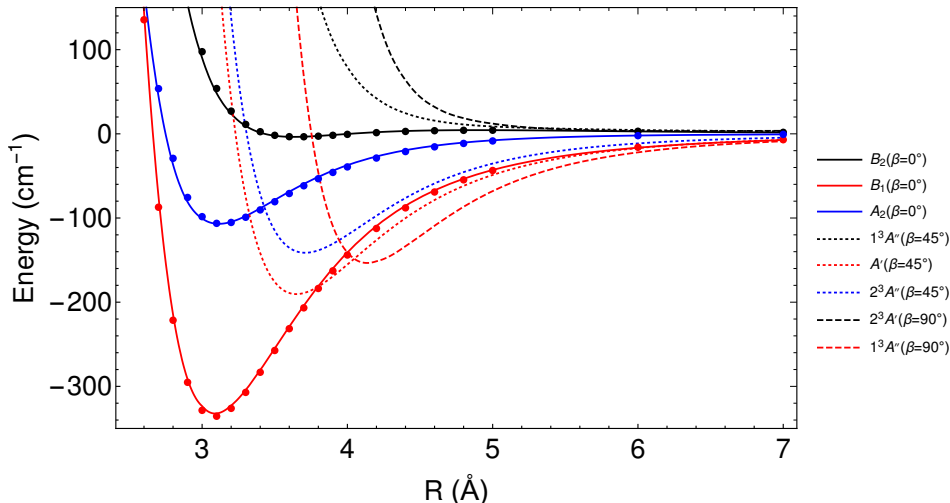


Figure 2. One-dimensional plots of the constructed $\text{CO}_2\text{-O}(^3P)$ potential energy surfaces for the selected angles: $\beta = 0^\circ$ (T-approach; solid lines), $\beta = 45^\circ$ (dotted lines), and $\beta = 90^\circ$ (dashed lines). *Ab-initio* points of de Lara-Castells et al. (2006) for $\beta = 0^\circ$ are shown (filled circles) for comparison. CO_2 geometry is fixed as linear.

cases when the symmetry of the system is increased are the T-approach ($\beta = 0^\circ$, symmetry group C_{2v}), and the colinear geometry ($\beta = 90^\circ$, symmetry group $C_{\infty v}$) (see de Lara-Castells et al. (2007) for details).

We first evaluated the interaction energies of the complex at the spin-restricted single and double coupled-cluster with perturbative triple excitations (RCCSD(T)) level of theory with the frozen core approximation on the augmented correlation-consistent polarized triple zeta (aug-cc-pVTZ) atomic basis. We also carried out explicitly correlated calculations with partially spin-adapted scheme (RCCSD(T)-F12) on a cc-pVTZ-F12 basis set (Knizia et al., 2009). Explicitly correlated calculations provide a dramatic improvement of the basis set convergence for coupled-cluster methods (Knizia et al., 2009). Scalar relativistic effects for the system were observable and accounted for using the Douglas-Kroll-Hess Hamiltonian (Wolf et al., 2002). To construct primitive surfaces, we kept the C-O internuclear distances frozen at their optimized equilibrium values ($r_{\text{CO}} = 1.167 \text{ \AA}$) while varying the distance R , of the approaching O atom to the center of mass of the CO_2 molecule, on a non-equidistant grid with the highest point density around the global surface minima (if applicable). An equidistant grid in angle β with steps of 10° was used. A total of about 200 *ab-initio* points per surface were evaluated using both methods. All calculations were carried out using MOLPRO2012 (Werner, Knowles, Knizia, Manby, Schütz, et al., 2012; Werner, Knowles, Knizia, Manby, & Schütz, 2012).

Final PESs were generated from the *ab-initio* points by constructing a fitting function of the form given by Sun et al. [2014] (Fig. 1). We obtained excellent agreement with the PESs reported by de Lara-Castells et al. (2006) (Fig. 2), with differences per energy point $< 1\%$ on average. We note that a common counterpoise technique (Boys & Bernardi, 1970) to compensate for basis set superposition errors did not play a significant role, likely due to the large basis sets used and fast convergence of the explicitly correlated methods. A detailed report of our investigation of the electronic structure of CO_3 complex, including its dependence on the bending angles, falls out of the scope of the present work and will be published elsewhere.

Table 1. Numerical parameters used in MOLSCAT production runs.

| Parameter | Value |
|------------|-----------------|
| j_{\max} | 100 |
| J_{\max} | 900 |
| JZCSMX | 8 |
| RMIN (Å) | 0.7 |
| RMAX (Å) | 30 ^a |
| STEPS | 12 |

^aAutomatic scaling with J was used.

2.2 Collisional Dynamics

We used MOLSCAT code (Hutson & Green, 1994) to calculate state-to-state quantum mechanical elastic and inelastic cross sections for the scattering problem $O(^3P) + CO_2(j) \rightarrow O(^3P) + CO_2(j')$, where the j and j' are the initial and final rotational quantum numbers of the CO_2 molecule, respectively. The set of time-independent coupled-channel Schrödinger equations was solved in close-coupling formalism with $CO_2(j)$ molecule represented as a rigid rotor with electronic interaction $O(^3P)$ described by our newly constructed potential energy surfaces (given in previous section). The complete scattering S -matrices, and differential and integral cross sections were calculated separately for each of the three triplet PESs and statistically averaged to obtain the final values.

We solved the scattering problem for 41 collision energy points on an equidistant grid between $E_{\text{col}} = 240 \text{ cm}^{-1}$ [$2.976 \times 10^{-2} \text{ eV}$] and $E_{\text{col}} = 40240 \text{ cm}^{-1}$ [4.9891 eV] in steps of 1000 cm^{-1} [0.124 eV]. The reduced mass $\mu = 11.73$ was used. Extensive testing was conducted to ensure the convergence with respect to the basis set size and numerical integration parameters. For the basis set consisting of rotational functions defined in terms of j_{\max} , the maximum allowed rotational quantum number of CO_2 molecule, we found that satisfactory convergence of the elastic cross sections can be achieved with a basis set as small as $j_{\max} = 30$. This remained true even when the centrifugal sudden (CS) approximation (McGuire & Kouri, 1974) was invoked to reduce the calculation size by approximating the transitions between rotational states higher than $\Delta j = 2$ (JZCSMX=2). Nevertheless, in order to ensure convergence of inelastic cross sections for initial rotational states j , present in the Maxwell-Boltzmann tail for the thermal upper atmosphere of Mars, we carried out production runs using a much larger basis set, with $j_{\max} = 100$ and JZCSMX=8. The convergence with respect to J , the total rotational quantum number of the complex, was achieved for $J_{\max} = 200 - 900$, where J_{\max} increases with collision energy.

Numerical integration was performed using modified log-derivative and hybrid modified log-derivative/Airy (LDA) propagators. We found that satisfactory precision could be achieved using a faster LDA scheme, with Airy propagator set up to automatically detect integration region boundaries. The parameters used in the production run are listed in Table 1. The computations took about 165 CPU-days.

3 Results and Analysis

3.1 Elastic and inelastic cross sections

For the three PESs, we calculated elastic and inelastic cross sections, $\sigma_{j,j'}(E)$, for the $O(^3P) + CO_2(j) \rightarrow O(^3P) + CO_2(j')$ scattering, where rotational quantum

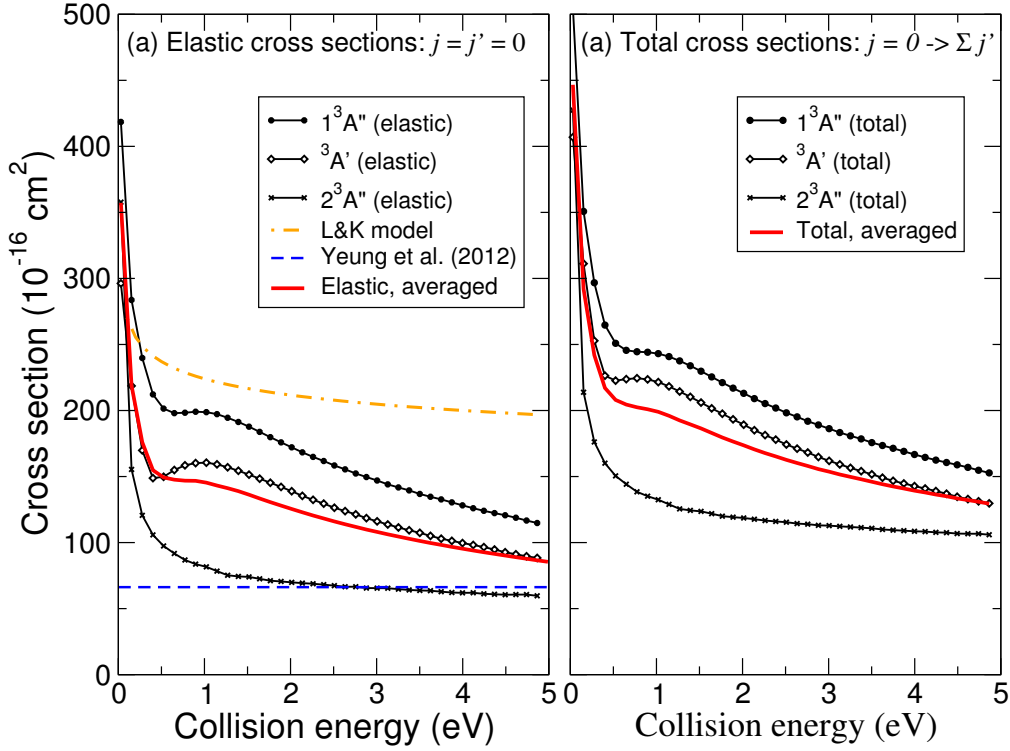


Figure 3. Cross sections for $O(^3P) + CO_2(j=0) \rightarrow O(^3P) + CO_2(j')$ scattering on three PESs: $1^3A''$ (circles), $3^3A'$ (diamonds), $2^3A''$ (crosses), and their statistically weighted average (solid line). *Left:* Elastic cross sections for $j=0$ compared to L&K model (Lewkow & Kharchenko, 2014) (dot-dashed) and hard-sphere cross section (Yeung et al., 2012) (dashed). *Right:* Total (elastic + inelastic) cross sections $\sigma_{j=0}(E) = \sum_{j'} \sigma_{j'}(E)$, where $j' = 0 \dots j_{\max}$.

numbers j and j' range from 0 to j_{\max} . The total cross sections are defined as

$$\sigma_j(E) = \sum_{j'} \sigma_{j,j'}(E), \quad (1)$$

where $j' = 0 \dots j_{\max}$. The cross sections are given in Fig. 3 as a function of the collision energy, $E = 0.03 - 5$ eV in the center-of-mass frame of reference, as well as in Table 2 for selected collision energies and rotational states.

With the exception of the lowest energy point ($E = 0.0297$ eV), our elastic cross sections, $\sigma_{0,0'}(E)$, are greater than estimated scattering cross sections of Yeung et al. (2012), who based their value on a Lennard-Jones interaction potential constructed on the lowest surface with estimated parameters, but smaller than the elastic cross sections of Lewkow and Kharchenko (2014) and than semi-empirical values used in numerous recent studies (Fox & Hać, 2014, 2018). Specifically, at $E = 0.5$ eV and $E > 4$ eV, our elastic cross sections appear to be smaller by more than 50% and 100%, respectively, than reported in the above studies. Our total cross sections are about 25% larger than the elastic cross sections, suggesting that internal (rotational) degrees of freedom of CO_2 molecule are significantly populated in collisions.

The relative significance of inelastic excitations is illustrated in Fig. 4, where we show cross sections $\sigma_{j=0,j'}(E)$ as a function of rotational quantum number j' for selected collision energies. Low-energy O atoms are 2-10 times more efficient at exciting low rotational states of CO_2 , but do not carry enough kinetic energy to excite high

Table 2. State-to-state cross sections $\sigma_{j=0,j'}(E)$ (units of 10^{-16} cm²) for selected energies.

| j' | Center-of-mass collision energy E (eV) | | | | | | | | |
|------------------|--|---------|---------|---------|---------|---------|---------|---------|-------|
| | 0.0297 | 0.154 | 0.28 | 0.53 | 0.77 | 1.51 | 2.5 | 3.5 | 4.0 |
| 0 | 357.16 | 218.851 | 175.952 | 146.854 | 145.377 | 136.222 | 116.021 | 101.273 | 95.37 |
| 2 | 40.858 | 25.328 | 20.963 | 15.329 | 13.266 | 10.877 | 8.609 | 7.512 | 7.122 |
| 4 | 14.632 | 9.308 | 7.779 | 4.616 | 3.974 | 3.294 | 2.78 | 2.489 | 2.426 |
| 6 | 9.495 | 6.425 | 5.182 | 3.433 | 3.084 | 2.686 | 2.484 | 2.389 | 2.367 |
| 8 | 6.674 | 4.799 | 3.94 | 2.663 | 2.426 | 2.083 | 1.838 | 1.801 | 1.815 |
| 10 | 4.23 | 3.094 | 2.417 | 1.862 | 1.713 | 1.628 | 1.457 | 1.369 | 1.367 |
| 12 | 2.918 | 2.701 | 2.497 | 2.093 | 1.942 | 1.74 | 1.586 | 1.477 | 1.452 |
| 14 | 2.91 | 2.61 | 2.337 | 1.798 | 1.683 | 1.413 | 1.304 | 1.275 | 1.265 |
| 16 | 2.11 | 2.101 | 1.739 | 1.36 | 1.258 | 1.173 | 1.056 | 1.017 | 0.983 |
| 18 | 1.96 | 1.988 | 1.799 | 1.521 | 1.415 | 1.406 | 1.311 | 1.18 | 1.142 |
| 20 | 1.721 | 1.838 | 1.645 | 1.291 | 1.37 | 1.289 | 1.051 | 0.994 | 0.941 |
| 22 | 0.901 | 1.581 | 1.354 | 1.052 | 1.128 | 1.014 | 0.933 | 0.87 | 0.868 |
| 24 | 0.31 | 1.564 | 1.443 | 1.252 | 1.16 | 1.21 | 1.049 | 0.984 | 0.947 |
| 26 | | 1.42 | 1.291 | 1.057 | 1.049 | 1.103 | 0.875 | 0.875 | 0.888 |
| 28 | | 1.051 | 1.009 | 0.848 | 0.974 | 0.92 | 0.761 | 0.74 | 0.716 |
| 30 | | 1.192 | 1.15 | 0.976 | 1.027 | 0.978 | 0.891 | 0.846 | 0.837 |
| 32 | | 1.1 | 1.076 | 0.853 | 0.822 | 0.878 | 0.785 | 0.736 | 0.712 |
| 34 | | 0.823 | 0.759 | 0.679 | 0.739 | 0.822 | 0.69 | 0.707 | 0.71 |
| 36 | | 0.647 | 0.78 | 0.788 | 0.918 | 0.852 | 0.818 | 0.812 | 0.772 |
| 38 | | 0.661 | 0.83 | 0.75 | 0.786 | 0.781 | 0.7 | 0.646 | 0.667 |
| 40 | | 0.636 | 0.702 | 0.594 | 0.613 | 0.72 | 0.668 | 0.627 | 0.618 |
| 42 | | 0.497 | 0.578 | 0.642 | 0.728 | 0.73 | 0.749 | 0.728 | 0.737 |
| 44 | | 0.408 | 0.608 | 0.668 | 0.702 | 0.684 | 0.793 | 0.692 | 0.701 |
| 46 | | 0.376 | 0.572 | 0.563 | 0.541 | 0.596 | 0.633 | 0.583 | 0.584 |
| 48 | | 0.282 | 0.474 | 0.53 | 0.557 | 0.653 | 0.687 | 0.681 | 0.688 |
| 50 | | 0.191 | 0.425 | 0.56 | 0.595 | 0.62 | 0.662 | 0.609 | 0.579 |
| 52 | | 0.148 | 0.443 | 0.498 | 0.511 | 0.504 | 0.594 | 0.579 | 0.59 |
| 54 | | 0.111 | 0.396 | 0.452 | 0.494 | 0.575 | 0.65 | 0.608 | 0.554 |
| 56 | | | 0.331 | 0.462 | 0.496 | 0.546 | 0.619 | 0.603 | 0.589 |
| 58 | | | 0.299 | 0.448 | 0.465 | 0.472 | 0.557 | 0.575 | 0.537 |
| 60 | | | 0.295 | 0.393 | 0.432 | 0.468 | 0.557 | 0.591 | 0.556 |
| 62 | | | 0.247 | 0.387 | 0.447 | 0.496 | 0.569 | 0.579 | 0.583 |
| 64 | | | 0.187 | 0.394 | 0.411 | 0.466 | 0.474 | 0.522 | 0.535 |
| 66 | | | 0.138 | 0.372 | 0.39 | 0.413 | 0.466 | 0.528 | 0.549 |
| 68 | | | 0.112 | 0.338 | 0.385 | 0.434 | 0.48 | 0.515 | 0.532 |
| 70 | | | 0.077 | 0.338 | 0.376 | 0.413 | 0.498 | 0.537 | 0.517 |
| 72 | | | 0.036 | 0.34 | 0.356 | 0.376 | 0.444 | 0.468 | 0.506 |
| 74 | | | 0.008 | 0.296 | 0.334 | 0.398 | 0.456 | 0.456 | 0.456 |
| 76 | | | | 0.264 | 0.317 | 0.418 | 0.429 | 0.447 | 0.45 |
| 78 | | | | 0.282 | 0.324 | 0.366 | 0.405 | 0.424 | 0.427 |
| 80 | | | | 0.275 | 0.332 | 0.348 | 0.407 | 0.442 | 0.471 |
| 82 | | | | 0.263 | 0.293 | 0.368 | 0.416 | 0.476 | 0.466 |
| 84 | | | | 0.248 | 0.273 | 0.343 | 0.392 | 0.394 | 0.389 |
| 86 | | | | 0.224 | 0.285 | 0.31 | 0.411 | 0.426 | 0.44 |
| 88 | | | | 0.235 | 0.276 | 0.326 | 0.422 | 0.427 | 0.447 |
| 90 | | | | 0.216 | 0.251 | 0.356 | 0.359 | 0.421 | 0.476 |
| 92 | | | | 0.208 | 0.268 | 0.289 | 0.372 | 0.47 | 0.448 |
| 94 | | | | 0.225 | 0.249 | 0.308 | 0.447 | 0.434 | 0.432 |
| 96 | | | | 0.195 | 0.272 | 0.359 | 0.346 | 0.357 | 0.359 |
| 98 | | | | 0.221 | 0.269 | 0.253 | 0.328 | 0.413 | 0.44 |
| 100 ^a | | | | 0.094 | 0.215 | 0.391 | 0.569 | 0.669 | 0.685 |

^aContributions from all $j' > 100$.

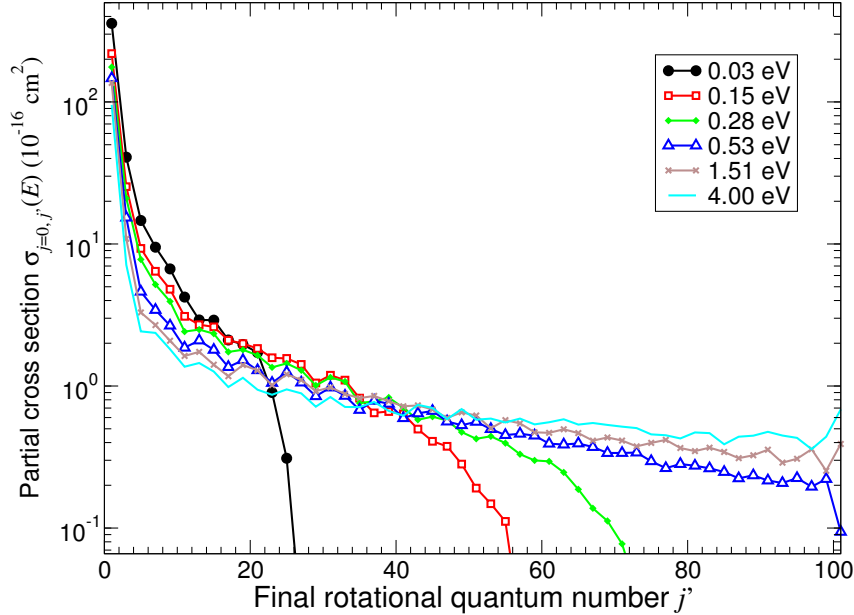


Figure 4. Cross sections $\sigma_{j=0,j'}(E)$ for $\text{O}(^3P) + \text{CO}_2(j=0) \rightarrow \text{O}(^3P) + \text{CO}_2(j')$ scattering on statistically averaged PES given as a function of j' for selected collision energies. Estimated uncertainties due to finite basis size are shown as residual values at $j' = 101$ (last point).

rotational states. This is consistent with general predictions of scattering theory where longer interaction times lead to more efficient energy transfer.

At collision energies smaller than about 0.5 eV, the rotational basis set is sufficiently large to fully capture the scattering dynamics (*i.e.*, the collision energies do not exceed the highest rotational energy included in the basis set), resulting in the cutoff in the rotational excitation spectrum. Estimated uncertainties due to the cutoff are shown as residual cross sections at $j' = 101$. For collision energies higher than about 0.5 eV, all rotational channels are collisionally populated and the approximate contributions from $j' > j_{\text{max}}$ are included in $\sigma_{j,j_{\text{max}}}(E)$. This approach allows us to estimate the uncertainties introduced by the finite basis size for $j_{\text{max}} = 100$ used in the production runs to be smaller than 0.1%, and largely negligible for low rotational levels (*e.g.*, $j' = 0 - 5$). For high rotational levels (*e.g.*, $j' > 15 - 20$), the uncertainty increases with collision energy and can be estimated to about 1-2% for $j' > 20 - 40$ and up to 10% at $j' = 90 - 100$ at $E > 4$ eV.

3.2 Differential cross sections

We have calculated state-to-state differential cross sections (DCSs) over the considered collision energy range separately for the three PESs for $\text{O}(^3P) + \text{CO}_2(j)$ scattering. The elastic DCSs, $Q_{j,j'}(\theta, E) = d\sigma_{j,j'}(\theta, E)/d\Omega$ and total DCSs, $Q_j(\theta, E) = \sum_{j'} d\sigma_{j,j'}(\theta, E)/d\Omega$, are illustrated in Fig. 5 for $j = 0$ in dependence on the center-of-mass collision energy E and the scattering angle θ . Here, $d\Omega = \sin\theta d\theta d\phi$ is the solid angle element and θ is defined as the angle between the initial and final trajectory of the incoming $\text{O}(^3P)$ atom, such that $\theta = 0^\circ$ corresponds to no deflection (T-approach), $\theta = 90^\circ$ to deflection collinear with the target CO_2 molecule, and $\theta = 180^\circ$ to full backscattering. 1D cuts for two collision energies, 0.0297 eV and 2.5 eV, representative of low- and high-energy scattering, are given in Fig. 6.

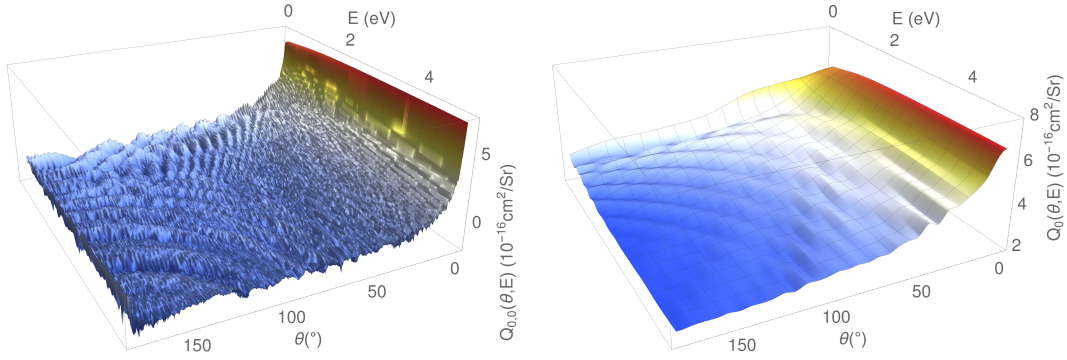


Figure 5. Elastic (left panel) and total (right panel) differential cross sections for $O(^3P) + CO_2(j = 0)$ scattering, statistically averaged over all PESs and presented in log scale.

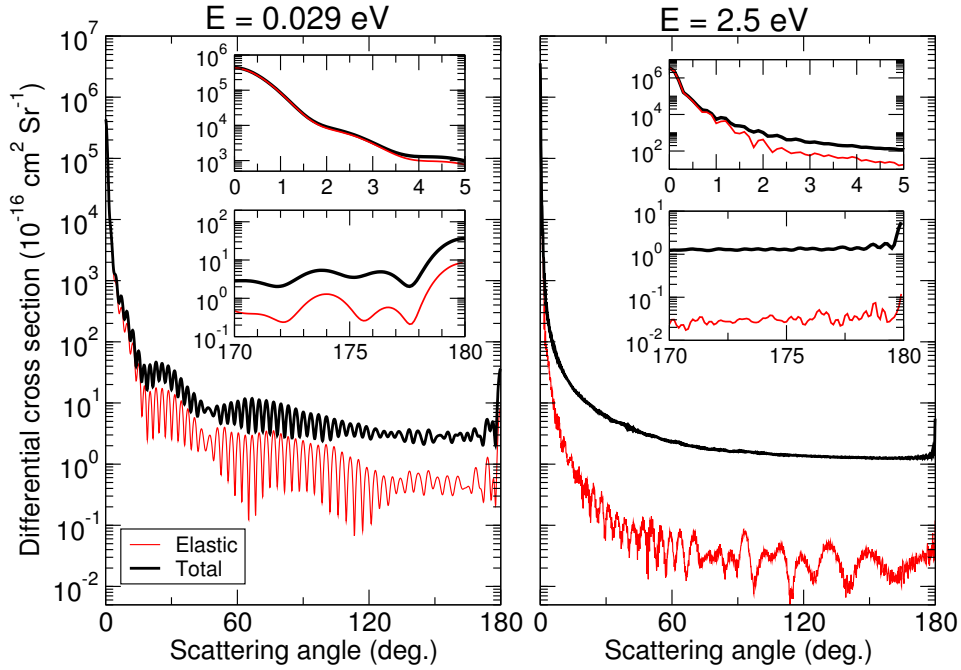


Figure 6. Elastic (thin red line) and total (thick black line) differential cross sections as functions of scattering angle shown for collision energies $E=0.0297$ eV (left panel) and $E=2.5$ eV (right panel). *Insets:* Zoom in on small and large scattering angles.

Both elastic and total DCSs are strongly anisotropic, with a dominant forward-scattering peak ($0^\circ < \theta < 2^\circ$ contributing to more than 90% of the integral cross section) and backscattering peaks clearly visible. Note that integral cross sections were calculated for the entire range of the scattering angle, $0^\circ < \theta < 180^\circ$. For small scattering angles θ , the DCSs are almost purely elastic, with inelastic excitations

appearing for $\theta > 3^\circ$ for low-energy collisions and for $\theta > 1^\circ$ for high-energy collisions (Fig. 6, inset). For larger scattering angles the total DCSs are about two orders of magnitude larger than the elastic DCSs, suggesting that rotational excitations are dominant, in particular at higher collision energies. The oscillatory structure present in elastic cross sections, in particular at low collision energies, is a real feature that does not average out because the number of participating partial waves is much smaller than in case of total DCSs, where both elastic and inelastic channels are included. At higher collision energies the number of contributing partial waves is much higher. Note that the values are calculated and shown in Fig. 4 for a single energy rather than averaged out over a realistic velocity distribution. At low collision energies several wave envelopes with maxima at scattering angles θ equal to about 30° , 70° , 100° , and 140° can be resolved. The complete dataset containing state-to-state CSs and DCSs is available (Gacesa et al., 2019).

3.3 Momentum transfer cross section

Momentum transfer (or momentum *transport*) cross section (MTCS) is an effective quantity suitable for modeling the average momentum transferred from a projectile to the target particle in a binary collision. MTCSs are used in studies of energy exchange, diffusion, and transport in non-thermal environments in astrophysics, atmospheric science, and aeronomy (Kharchenko et al., 1997; Zhang et al., 2009).

For $O(^3P) + CO_2(j = 0) \rightarrow O(^3P) + CO_2(j' = 0)$ elastic scattering, the momentum transfer cross section is given by

$$\sigma_{j=0}^{\text{mt}}(E) = \int_0^\infty Q_{0,0}(\theta, E) \sin \theta (1 - \cos \theta) d\theta, \quad (2)$$

where $Q_{0,0}(\theta, E)$ is the differential cross section for $j = j' = 0$. Following Eq. (2), we have calculated MTCSs as a function of collision energy independently for each PES, as well as their statistically weighted average (Fig. 7).

Computed MTCSs are on average less than 1% of the elastic and total cross sections, except for low energy collisions, indicating that energy transfer from superthermal O to thermal CO_2 background is rather inefficient (Fig. 7, *inset*) even in comparison with $O(^3P)+H_2$ collisions where MTCSs are greater than 2% (Gacesa et al., 2012). In comparison, in the same collision energy range, MTCSs for atom-atom collisions tend to be about 10%-25% of the total cross sections between a heavy projectile and a light target species such as N+He, and about 2%-18% for heavy species, such as N+Ar (Zhang et al., 2008). The evaluated MTCSs have direct consequences on Mars aeronomy and atmospheric escape, where we can expect larger escape fluxes of non-thermal atomic oxygen produced at lower altitudes (Lillis et al., 2017), and possibly other atomic species, such as C and N, escaping through a thick layer of CO_2 .

4 Summary and Discussion

We have carried out a theoretical study of $O(^3P) + CO_2 \rightarrow O(^3P) + CO_2$ non-reactive scattering at thermal and superthermal collision energies up to 5 eV in the center-of-mass frame. The selected energy range is typical in non-thermal-equilibrium conditions in upper planetary atmospheres exposed to solar radiation and plasma inputs. To describe the electronic interactions between the colliding particles, we have constructed *ab-initio* potential energy surfaces for three electronic states correlating to the energetically-lowest asymptote of the $O(^3P)-CO_2(^1\Sigma^+)$ complex. The surfaces were constructed in a restricted planar geometry, with the CO_2 molecule assumed to be linear with C-O internuclear separation fixed at the equilibrium distance.

With the PESs as inputs, we computed velocity-dependent state-to-state and total elastic and inelastic cross sections, corresponding differential cross sections, as

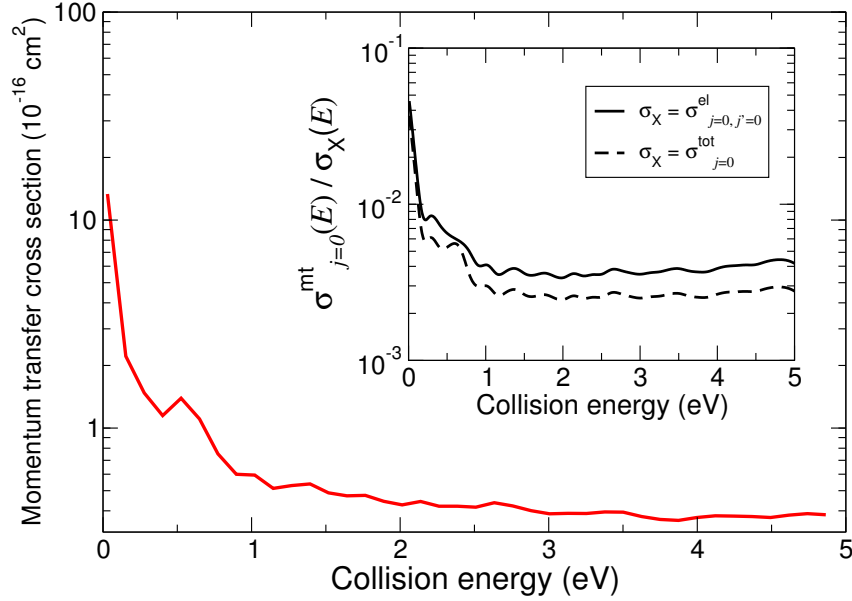


Figure 7. Momentum transfer cross section $\sigma_{j=0}^{\text{mt}}(E)$ for $\text{O}(^3P) + \text{CO}_2(j=0)$ as a function of collision energy statistically averaged over three PESs. *Inset:* Ratio of the MTCS and elastic and total cross sections, respectively, for the same initial state.

well as elastic momentum transfer cross sections. The CO_2 molecule was modeled as a rigid rotor and rotational-vibrational couplings between the symmetric, bending, and asymmetric vibrational modes were not included in the production run of the model. The scattering problem was described using a quantum mechanical coupled-channel formalism and solved numerically. Thus, the cross sections and derived physical quantities were constructed from first principles without any external empirical parameters. Although computationally intensive, the ab initio approach has several major advantages over classical theory, such as evaluation of all state-to-state transitions induced by collisions and more complete treatment of purely quantum effects, expected to play a significant role in improving the predictive power and precisions of models (Kao et al., 2019).

Our computed elastic cross sections are smaller than the elastic cross sections estimated by mass-scaling from well-described atom-molecule systems (Lewkow & Kharchenko, 2014; Fox & Hać, 2018), but larger than a Lennard-Jones cross section reported by Yeung et al. (2012). Specifically, at superthermal energies, our elastic cross sections range between $1.5 \times 10^{-14} \text{ cm}^2$ at about 1 eV collision energy, down to $8.5 \times 10^{-15} \text{ cm}^2$ at 5 eV. In comparison, the widely used elastic cross sections of Lewkow and Kharchenko (2014) evaluate to $2.24 \times 10^{-14} \text{ cm}^2$ and $1.97 \times 10^{-14} \text{ cm}^2$ for the two collision energies, respectively. Calculated differential cross sections (DCSs) are strongly favoring forward scattering with the anisotropy increasing with the collision energy. The small-angle forward scattering is mostly elastic with negligible kinetic energy transfer to internal degrees of freedom of the CO_2 molecule. In contrast, for larger scattering angles the inelastic DCSs are nearly two orders of magnitude greater than elastic ones, indicating that the kinetic energy transfer to internal excitations is rather efficient. For the highest collision energies considered, the total inelastic CS is equal to approximately one half of the elastic CS, suggesting that up to 50% of the translational kinetic energy of the $\text{O}(^3P)$ atom is converted into internal excitations (rotations) of the CO_2 molecule. Yeung et al. (2012) observed significant energy

transfer in the $O(^3P) + CO_2$ system, with “an average of only 41% of the collision energy remaining in product translation”. A simple statistical estimate based on level energies puts that number as high as 75% (Fox & Hać, 2018). In comparison, in $O(^3P)+CO$ collisions, on average 84% of the energy remains in product translation, approximately 80% is retained in Ar + ethane collisions, and 60% in superthermal $O(^3P)+C_2H_6$ collisions. Yeung et al. (2012) suggested that such a large fraction of kinetic energy transfer to inelastic excitations may be due to significant contribution from a short-lived intermediate CO_3 complex that can form in the collisions and yield reaction products corresponding to inelastic scattering of $O(^3P)+CO_2$.

The most significant contribution to the uncertainties in the calculated cross sections comes from approximating the CO_2 molecule with a linear rigid rotor. With vibrational modes and rotational-vibrational coupling included in the model, we expect our inelastic (and total) scattering cross sections to be lower than what nature intended because of absence of direct kinetic energy transfer into vibrations. The effects should be more significant at the high-end of the collision energy range considered, above about 4 eV, where the vibrational excitations were predicted to overtake rotational excitations as a dominant inelastic process (Schatz & Redmon, 1981). Based on energy transfer arguments and reported vibrational cross sections in existing studies, we can estimate the uncertainties in calculated cross sections. If we assume that 65% of translational energy is, indeed, converted into the internal excitations of CO_2 molecule in a collision at $E = 4.3$ eV (Yeung et al., 2012), our total cross sections should be greater by about 13%, or $\sigma_{j=0} \approx 1.5 \times 10^{-14}$ cm². At lower collision energies, the uncertainties would be proportionally smaller.

In comparison, a theoretical study of vibrational excitations in the title process based on the infinite-order-sudden (IOS) approximation (Mullaney Harvey, 1982) reported cross sections for collisionally exciting $CO_2(01^1_0)$ (first bending mode) greater than 5.6×10^{-17} cm² at $E > 2$ eV, or less than 1% of our elastic cross sections. Upschulte and Caledonia (1992) measured the cross sections for O-atom excitation of $CO_2(00^0_1)$ mode at $E = 3.9$ eV (8 km/s) to be equal to 3.7×10^{-18} cm² and recommended a value of 6.4×10^{-17} cm² as a cross section for O-atom excitation of $CO_2(01^1_0)$. Their proposed values are in good agreement with a quasi-classical trajectory (QCT) study of collisional excitation of $CO_2(NN'1)$, where N and N' correspond to excited symmetric and bending vibrational modes, respectively (Schatz & Redmon, 1981). These studies suggest that the cross sections for collisionally exciting the lowest antisymmetric vibrational mode of CO_2 are, at best, nearly two orders of magnitude smaller than our inelastic (rotational) cross sections. If we assume that the total inelastic cross section for vibrational excitations scales linearly with the number of open channels (vibrational states), we can make a more direct comparison with our results. At collision energy $E = 3.9$ eV, lowest 14 antisymmetric vibrational modes, up to $v_a = 13$, can be excited, yielding a total vibrational cross section 8.3×10^{-16} cm² for $CO_2(NN', 13)$, or about one half of the value estimated from the translational energy fractions alone. Note that the estimated fraction of the translational energy transferred to the internal excitations by Yeung et al. (2012) is rather high.

The elastic cross sections are less likely to be significantly affected by the absence of vibrational excitations in our model. We tested the convergence of scattering calculations for basis sets comprised of as few as six internal states ($j'_{\max} = 5$), or of only 5-10 bending mode energies ($E_b = 667$ cm⁻¹) with rotational states modeled using the IOS approximation. The elastic cross sections computed with these minimal basis sets were about 20% larger than our production values, while a basis set with as few as 30 rotational states matched the production values within 2%. However, matching the production inelastic cross sections required large basis sets.

Three final points should be mentioned. First, deviation from the linear geometry (bending angle $\beta \neq 180^\circ$) will likely have an effect on the cross sections. de Lara-

Castells et al. (2006) constructed PESs for the bending angles $150^\circ < \beta < 210^\circ$ and demonstrated that for $\beta < 180^\circ$, for which the CO₂ molecule bends towards the incoming O(³P) atom, the surfaces are more attractive with deeper wells, while the opposite is true for $\beta > 180^\circ$. However, since the binding angle is directly connected to the strength of rotational-vibrational couplings, it is difficult to assess the effects of geometry changes without conducting further studies with vibrational degrees of freedom included in the model. Our preliminary calculations match well the PESs of de Lara-Castells et al. (2006) and the work to extend the scattering model to include vibrations is in progress. Second, even though we conducted the scattering calculations on three PESs correlating to the lowest energy asymptote of O(³P) + CO₂ complex, we did not take into account intersurface couplings that could lead to surface hopping. Such studies were conducted for spin-orbit couplings at lower collision energies (de Lara-Castells et al., 2007) and the impact of surface hopping on scattering cross sections were analyzed for other systems (Maiti & Schatz, 2003; Li & Han, 2009; Gacesa & Kharchenko, 2014). Based on these studies, we estimate that for high collision energies considered in this study at current level of theory, the intersystem crossing effects are not likely to significantly affect the final results. Third, we note that reactive processes were not considered in this study. Yeung et al. (2012) calculated the branching fractions for nonreactive scattering to be 0.984, as compared to the oxygen-atom abstraction reaction (4×10^{-6}) and O atom exchange (0.016), with the uncertainties of about 30% cited for all processes. Thus, we estimate that neglecting nonreactive channels contributes to no more than 2% uncertainties in the reported cross sections.

Acknowledgments

This study has been partially funded NASA, grant #17-MDAP17.2-0152. The authors are grateful to J. Fox, Y. Lee, and B. Jakosky for helpful suggestions and discussion, and to M.-P. de Lara-Castells for sharing with us a digital version of their potential energy surface points. The complete dataset containing state-to-state CSs and DCSs and Fortran subroutines to generate potential energy surfaces are available online (Gacesa et al., 2019).

References

- Amerstorfer, U. V., Gröller, H., Lichtenegger, H., Lammer, H., Tian, F., Noack, L., ... Güdel, M. (2017, June). Escape and evolution of Mars's CO₂ atmosphere: Influence of suprathreshold atoms. *Journal of Geophysical Research: Planets*, *122*, 1321-1337. doi: 10.1002/2016JE005175
- Balakrishnan, N., Kharchenko, V., & Dalgarno, A. (1998, October). Slowing of energetic O(³P) atoms in collisions with N₂. *Journal of Geophysical Research*, *1032*, 23393-23398. doi: 10.1029/98JA02198
- Bass, J. N. (1974, April). Translation to vibration energy transfer in O + NH₃ and O + CO₂ collisions. *Journal of Chemical Physics*, *60*, 2913-2921. doi: 10.1063/1.1681461
- Billing, G. D., & Clary, D. C. (1983, October). Semiclassical calculation of energy transfer in polyatomic molecules. IX. Cross sections for M + CO₂ (000) → M + CO₂(nml) (M = He and Ar). *Chemical Physics*, *80*, 213-219. doi: 10.1016/0301-0104(83)85274-4
- Bovino, S., Zhang, P., Gianturco, F. A., Dalgarno, A., & Kharchenko, V. (2011, January). Energy transfer in O collisions with He isotopes and Helium escape from Mars. *Geophysical Research Letters*, *38*, L02203. doi: 10.1029/2010GL045763
- Boys, S. F., & Bernardi, F. (1970). The calculation of small molecular interactions by the differences of separate total energies. Some procedures with reduced

- errors. *Molecular Physics*, *19*(4), 553–566.
- Castle, K. J., Black, L. A., Simone, M. W., & Dodd, J. A. (2012, April). Vibrational relaxation of $\text{CO}_2(\nu_2)$ by $\text{O}(^3\text{P})$ in the 142-490 K temperature range. *Journal of Geophysical Research: Space Physics*, *117*, A04310. doi: 10.1029/2012JA017519
- Castle, K. J., Kleissas, K. M., Rhinehart, J. M., Hwang, E. S., & Dodd, J. A. (2006, September). Vibrational relaxation of $\text{CO}_2(\nu_2)$ by atomic oxygen. *Journal of Geophysical Research: Space Physics*, *111*, A09303. doi: 10.1029/2006JA011736
- Cecchini, M. R., & Castle, K. J. (2015, October). Vibrational relaxation of $^{13}\text{CO}_2(\nu_2)$ by atomic oxygen. *Chemical Physics Letters*, *638*, 149-152. doi: 10.1016/j.cplett.2015.08.051
- Cipriani, F., Leblanc, F., & Berthelier, J. J. (2007, July). Martian corona: Non-thermal sources of hot heavy species. *Journal of Geophysical Research: Planets*, *112*, E07001. doi: 10.1029/2006JE002818
- de Lara-Castells, M. P., Hernández, M. I., Delgado-Barrio, G., Villarreal, P., & López-Puertas, M. (2006, April). Vibrational quenching of $\text{CO}_2(010)$ by collisions with $\text{O}(^3\text{P})$ at thermal energies: A quantum-mechanical study. *Journal of Chemical Physics*, *124*(16), 164302-164302. doi: 10.1063/1.2189860
- de Lara-Castells, M. P., Hernández, M. I., Delgado-Barrio, G., Villarreal, P., & López-Puertas, M. (2007). Key role of spin-orbit effects in the relaxation of $\text{CO}_2(010)$ by thermal collisions with $\text{O}(^3P_j)$. *Molecular Physics*, *105*, 1171-1181. doi: 10.1080/00268970701244809
- Feofilov, A. G., Kutepov, A. A., She, C.-Y., Smith, A. K., Pesnell, W. D., & Goldberg, R. A. (2012, October). $\text{CO}_2(\nu_2)$ -O quenching rate coefficient derived from coincidental SABER/TIMED and Fort Collins lidar observations of the mesosphere and lower thermosphere. *Atmospheric Chemistry & Physics*, *12*, 9013-9023. doi: 10.5194/acp-12-9013-2012
- Fox, J. L., & Hać, A. B. (2009, December). Photochemical escape of oxygen from Mars: A comparison of the exobase approximation to a Monte Carlo method. *Icarus*, *204*, 527-544. doi: 10.1016/j.icarus.2009.07.005
- Fox, J. L., & Hać, A. B. (2014, January). The escape of O from Mars: Sensitivity to the elastic cross sections. *Icarus*, *228*, 375-385. doi: 10.1016/j.icarus.2013.10.014
- Fox, J. L., & Hać, A. B. (2018, January). Escape of $\text{O}(^3\text{P})$, $\text{O}(^1\text{D})$, and $\text{O}(^1\text{S})$ from the Martian atmosphere. *Icarus*, *300*, 411-439. doi: 10.1016/j.icarus.2017.08.041
- Gacesa, M., & Kharchenko, V. (2014, October). Quantum reactive scattering of $\text{O}(^3\text{P})+\text{H}_2$ at collision energies up to 4.4 eV. *Journal of Chemical Physics*, *141*(16), 164324. doi: 10.1063/1.4899179
- Gacesa, M., Lewkow, N., & Kharchenko, V. (2017, March). Non-thermal production and escape of OH from the upper atmosphere of Mars. *Icarus*, *284*, 90-96. doi: 10.1016/j.icarus.2016.10.030
- Gacesa, M., Lillis, R. J., & Zahnle, K. J. (2019, Jun). *O(3P)+CO2 scattering cross sections at superthermal collision energies for planetary aeronomy: Raw data pre-release (v0.9-beta)*. GitHub repository referenced on Zenodo. Retrieved from <https://doi.org/10.5281/zenodo.3256699> doi: 10.5281/zenodo.3256699
- Gacesa, M., Zhang, P., & Kharchenko, V. (2012, May). Non-thermal escape of molecular hydrogen from Mars. *Geophysical Research Letters*, *39*, L10203. doi: 10.1029/2012GL050904
- Garrett, B. C. (1984, June). Basis-set effects in quantum-mechanical calculations of translational-to-vibrational energy transfer in $\text{O}(^3\text{P}) + \text{CO}_2$ collisions. *Chemical Physics*, *87*, 63-71. doi: 10.1016/0301-0104(84)85139-3
- Hunten, D. M., & Donahue, T. M. (1976). Hydrogen loss from the terrestrial plan-

- ets. *Annual Review of Earth and Planetary Sciences*, 4, 265-292. doi: 10.1146/annurev.earth.04.050176.001405
- Hutson, J. M., & Green, S. (1994). *MOLSCAT Version 14, Collaborative Computational Project 6 (Daresbury Laboratory: UK Engineering and Phys. Sci. Res. Council)*. Retrieved from <http://www.giss.nasa.gov/tools/molscat/>
- Jakosky, B. M., Brain, D., Chaffin, M., Curry, S., Deighan, J., Grebowsky, J., ... Zurek, R. (2018, November). Loss of the Martian atmosphere to space: Present-day loss rates determined from MAVEN observations and integrated loss through time. *Icarus*, 315, 146-157. doi: 10.1016/j.icarus.2018.05.030
- Jakosky, B. M., Lin, R. P., Grebowsky, J. M., Luhmann, J. G., Mitchell, D. F., Beutelschies, G., ... Zurek, R. (2015, December). The Mars Atmosphere and Volatile Evolution (MAVEN) Mission. *Space Science Reviews*, 195, 3-48. doi: 10.1007/s11214-015-0139-x
- Kallio, E., Chaufray, J.-Y., Modolo, R., Snowden, D., & Winglee, R. (2011, December). Modeling of Venus, Mars, and Titan. *Space Science Reviews*, 162, 267-307. doi: 10.1007/s11214-011-9814-8
- Kao, D.-Y., Gacesa, M., Wentzcovitch, R. M., Domagal-Goldman, S., Kopparapu, R. K., Klippenstein, S. J., ... Fortney, J. J. (2019, May). Impacts of Quantum Chemistry Calculations on Exoplanetary Science, Planetary Astronomy, and Astrophysics. In *Bulletin of the American Astronomical Society* (Vol. 51, p. 240).
- Kharchenko, V., Dalgarno, A., Zygelman, B., & Yee, J.-H. (2000, November). Energy transfer in collisions of oxygen atoms in the terrestrial atmosphere. *Journal of Geophysical Research*, 105, 24899-24906. doi: 10.1029/2000JA000085
- Kharchenko, V., Tharamel, J., & Dalgarno, A. (1997, January). Kinetics of thermalization of fast nitrogen atoms beyond the hard sphere approximation. *J. Atmospheric Sol.-Terr. Phys.*, 59. doi: 10.1016/S1364-6826(96)00081-8
- Knizia, G., Adler, T. B., & Werner, H.-J. (2009). Simplified CCSD(T)-F12 methods: Theory and benchmarks. *Journal of Chemical Physics*, 130(5), 054104.
- Lammer, H. (2013). *Origin and Evolution of Planetary Atmospheres*. doi: 10.1007/978-3-642-32087-3
- Lammer, H., Kolb, C., Penz, T., Amerstorfer, U. V., Biernat, H. K., & Bodis-elitsch, B. (2003, July). Estimation of the past and present Martian water-ice reservoirs by isotopic constraints on exchange between the atmosphere and the surface. *International Journal of Astrobiology*, 2, 195-202. doi: 10.1017/S1473550403001605
- Leblanc, F., Benna, M., Chaufray, J. Y., Martinez, A., Lillis, R., Curry, S., ... Jakosky, B. (2019). First in situ evidence of Mars nonthermal exosphere. *Geophysical Research Letters*, 46(8), 4144-4150. doi: 10.1029/2019GL082192
- Leblanc, F., Chaufray, J. Y., Modolo, R., Leclercq, L., Curry, S., Luhmann, J., ... Jakosky, B. (2017, December). On the Origins of Mars' Exospheric Non-thermal Oxygen Component as Observed by MAVEN and Modeled by HELIOSARES. *Journal of Geophysical Research: Planets*, 122, 2401-2428. doi: 10.1002/2017JE005336
- Lee, Y., Combi, M. R., Tenishev, V., Bougher, S. W., Deighan, J., Schneider, N. M., ... Jakosky, B. M. (2015, November). A comparison of 3-D model predictions of Mars' oxygen corona with early MAVEN IUVS observations. *Geophysical Research Letters*, 42, 9015-9022. doi: 10.1002/2015GL065291
- Lee, Y., Combi, M. R., Tenishev, V., Bougher, S. W., & Lillis, R. J. (2015, November). Hot oxygen corona at Mars and the photochemical escape of oxygen: Improved description of the thermosphere, ionosphere, and exosphere. *J. Geophys. Res.*, 120, 1880-1892. doi: 10.1002/2015JE004890
- Lewkow, N. R., & Kharchenko, V. (2014, August). Precipitation of Energetic Neutral Atoms and Induced Non-thermal Escape Fluxes from the Martian Atmosphere. *Astrophysics Journal*, 790, 98. doi: 10.1088/0004-637X/790/2/98

- Li, B., & Han, K.-L. (2009, September). Mixed Quantum-Classical Study of Nonadiabatic Dynamics in the $O(^3P_{2,1,0}, ^1D_2) + H_2$ Reaction. *Journal of Physical Chemistry A*, *113*, 10189-10195. doi: 10.1021/jp904727d
- Lillis, R. J., Brain, D. A., Bougher, S. W., Leblanc, F., Luhmann, J. G., Jakosky, B. M., ... Lin, R. P. (2015, December). Characterizing Atmospheric Escape from Mars Today and Through Time, with MAVEN. *Space Science Reviews*, *195*, 357-422. doi: 10.1007/s11214-015-0165-8
- Lillis, R. J., Deighan, J., Fox, J. L., Bougher, S. W., Lee, Y., Combi, M. R., ... Chaufray, J.-Y. (2017, March). Photochemical escape of oxygen from Mars: First results from MAVEN in situ data. *Journal of Geophysical Research: Space Physics*, *122*, 3815-3836. doi: 10.1002/2016JA023525
- Liu, S. C., & Donahue, T. M. (1975, February). The aeronomy of the upper atmosphere of Venus. *Icarus*, *24*, 148-156. doi: 10.1016/0019-1035(75)90092-5
- Liu, S. C., & Donahue, T. M. (1976, June). The regulation of hydrogen and oxygen escape from Mars. *Icarus*, *28*, 231-246. doi: 10.1016/0019-1035(76)90035-X
- Maiti, B., & Schatz, G. C. (2003, December). Theoretical studies of intersystem crossing effects in the $O(^3P, ^1D)+H_2$ reaction. *Journal of Chemical Physics*, *119*, 12360-12371. doi: 10.1063/1.1623481
- McGuire, P., & Kouri, D. J. (1974). Quantum mechanical close coupling approach to molecular collisions. jz-conserving coupled states approximation. *Journal of Chemical Physics*, *60*(6), 2488-2499.
- Mullaney Harvey, N. (1982, May). A quantum mechanical investigation of vibrational energy transfer in $O(^3P) + CO_2$ collisions. *Chemical Physics Letters*, *88*, 553-558.
- Schatz, G. C., & Redmon, M. J. (1981). A quasiclassical trajectory study of collisional excitation in $O(^3P)+CO_2$. *Chemical Physics*, *58*(2), 195-201.
- Sharma, R. D., & Wintersteiner, P. P. (1990). Role of carbon dioxide in cooling planetary thermospheres. *Geophysical Research Letters*, *17*(12), 2201-2204.
- Shematovich, V. I. (2017, July). Suprathermal oxygen atoms in the Martian upper atmosphere: Contribution of the proton and hydrogen atom precipitation. *Solar System Research*, *51*, 249-257. doi: 10.1134/S0038094617040050
- Suzukawa Jr, H. H., Wolfsberg, M., & Thompson, D. L. (1978). A quasiclassical trajectory study of the energy transfer in CO_2 -rare gas systems. *Journal of Chemical Physics*, *68*(2), 455-472.
- Thiemens, M. H., Chakraborty, S., & Jackson, T. L. (2014). Decadal $\Delta^{17}O$ record of tropospheric CO_2 : Verification of a stratospheric component in the troposphere. *Journal of Geophysical Research: Atmospheres*, *119*(10), 6221-6229.
- Thiemens, M. H., Jackson, T. L., & Brenninkmeijer, C. A. (1995). Observation of a mass independent oxygen isotopic composition in terrestrial stratospheric CO_2 , the link to ozone chemistry, and the possible occurrence in the Martian atmosphere. *Geophysical Research Letters*, *22*(3), 255-257.
- Upschulte, B. L., & Caledonia, G. E. (1992, February). Laboratory measurements of infrared excitation cross sections of fast O-atom collisions with CO, CO_2 , and CH_4 . *Journal of Chemical Physics*, *96*, 2025-2033. doi: 10.1063/1.462105
- Uudus, N., Magaki, S., & Balakrishnan, N. (2005, January). Quantum mechanical investigation of rovibrational relaxation of H_2 and D_2 by collisions with Ar atoms. *Journal of Chemical Physics*, *122*(2), 024304. doi: 10.1063/1.1829976
- Werner, H.-J., Knowles, P. J., Knizia, G., Manby, F. R., & Schütz, M. (2012). MOLPRO: a generalpurpose quantum chemistry program package. *WIREs Computational Molecular Science*, *2*, 242-253.
- Werner, H.-J., Knowles, P. J., Knizia, G., Manby, F. R., Schütz, M., Celani, P., ... Wang, M. (2012). *MOLPRO, version 2012.1, a package of ab initio programs*. Cardiff, UK. (see <http://www.molpro.net>)
- Wiegel, A. A., Cole, A. S., Hoag, K. J., Atlas, E. L., Schauffler, S. M., & Boering, K. A. (2013). Unexpected variations in the triple oxygen isotope composi-

- tion of stratospheric carbon dioxide. *Proceedings of the National Academy of Sciences*, *110*(44), 17680–17685.
- Wolf, A., Reiher, M., & Hess, B. A. (2002). The generalized douglas–kroll transformation. *Journal of Chemical Physics*, *117*(20), 9215–9226.
- Yeung, L. Y., Okumura, M., Zhang, J., Minton, T. K., Paci, J. T., Karton, A., . . . Schatz, G. C. (2012, January). O(³P) + CO₂ Collisions at Hyperthermal Energies: Dynamics of Nonreactive Scattering, Oxygen Isotope Exchange, and Oxygen-Atom Abstraction. *Journal of Physical Chemistry A*, *116*, 64–84. doi: 10.1021/jp2080379
- Zahnle, K., Haberle, R. M., Catling, D. C., & Kasting, J. F. (2008, November). Photochemical instability of the ancient Martian atmosphere. *Journal of Geophysical Research: Planets*, *113*, E11004. doi: 10.1029/2008JE003160
- Zhang, P., Kharchenko, V., Dalgarno, A., Matsumi, Y., Nakayama, T., & Takahashi, K. (2008, Mar). Approach to thermal equilibrium in atomic collisions. *Physical Review Letters*, *100*, 103001. Retrieved from <https://link.aps.org/doi/10.1103/PhysRevLett.100.103001> doi: 10.1103/PhysRevLett.100.103001
- Zhang, P., Kharchenko, V., Jamieson, M. J., & Dalgarno, A. (2009, July). Energy relaxation in collisions of hydrogen and deuterium with oxygen atoms. *Journal of Geophysical Research*, *114*, A07101. doi: 10.1029/2009JA014055